

(Electronic Supplementary Information)

Molecular mechanism of methane dry reforming on $\text{Co}_3\text{Mo}_3\text{N}$ catalyst with dual sites

Narges Manavi, Bin Liu*

Tim Taylor Department of Chemical Engineering, Kansas State University, Manhattan, KS, 66506

* Corresponding author: Tel: 785-532-4331. Email: binliu@ksu.edu

FIGURE LIST

Fig. S1. Optimized structures of the intermediates listed in Table 2 on Co(0001). C, O, H, and Co are depicted in brown, red, light pink, and dark blue, respectively.

Fig. S2. Optimized structures of the intermediates listed in Table 2 on Mo₂N(110). C, O, H, Mo, and N are depicted in brown, red, light pink, dark blue, and light blue, respectively.

Fig. S3. Optimized transition state structures on Co(0001). Atomic distances (in Å) are labeled and indicated in dashed lines. C, O, H, and Co are depicted in brown, red, white, and dark blue, respectively.

Fig. S4. Optimized transition state structures on Mo-terminated Mo₂N(110). Atomic distances (in Å) are labeled and indicated in dashed lines. C, O, H, Mo, and N are depicted in brown, red, white, pink, and light blue, respectively.

Fig. S5. Free energy profiles depicting on Co₃Mo₃N(111) (black), Co(0001) (red dashed), and Mo₂N(110) (blue dotted) emphasizing the CH₄ activation and COH oxidation pathway at 1000 K and 1 bar. Gas phase CO₂ and CH₄ and corresponding clean surfaces were used as the zero energy references. Similarly, gas phase CO and H₂, following the reaction stoichiometry, are considered as the final products. The kinetically critical C–H activation step and carbon formation are highlighted with grey bars. The inset figure illustrates the accompanying CO₂ dissociation on respective Co₃Mo₃N(111) (black), Co(0001) (red dashed), and Mo₂N(110) (blue dotted) surfaces under the same condition.

Fig. S6. Optimized transition states for CH₄ activation on transition metal surfaces. The distances (in Å) of the dissociating C–H bond are labeled and indicated in dashed lines.

Fig. S7. Linear scaling relations of the binding energy corresponding to fragments bound in the most stable adsorption site for (a) H versus C/O, (b) CH versus C, (c) CO versus O, (d) OH versus O. The standard deviations, MAE, and MAX are also shown.

Fig. S8. BEP relationship for CH₄ C–H bond activation in terms of dissociation energies (ΔE) and energy barriers (E_a). The standard deviations, MAE, and MAX are also shown.

TABLE LIST

Table S1. Lattice parameters of surface models.

Table S2. Binding energies (eV) of H, CH₃ on their preferred binding sites of the close-packed transition metal surfaces; CH₄ dissociation energies (ΔE); and C–H bond activation energy barriers (E_a). Literature values are shown in the parentheses.

Table S3. Rate constants of the elementary DRM steps on Co₃Mo₃N(111), Co(0001), Mo₂N(110), and Ni(111). The elementary step indices correspond to the mechanism shown in Table 2 of the main text.

Table S4. Rate constants and equilibrium constants on Co₃Mo₃N(111), Ni(111), Co(0001), and Mn₂N(110) used in Eqns. (S3, S4, S6, S7).

Appendix 1. Derivations of single-site and dual-site microkinetic models for DRM.

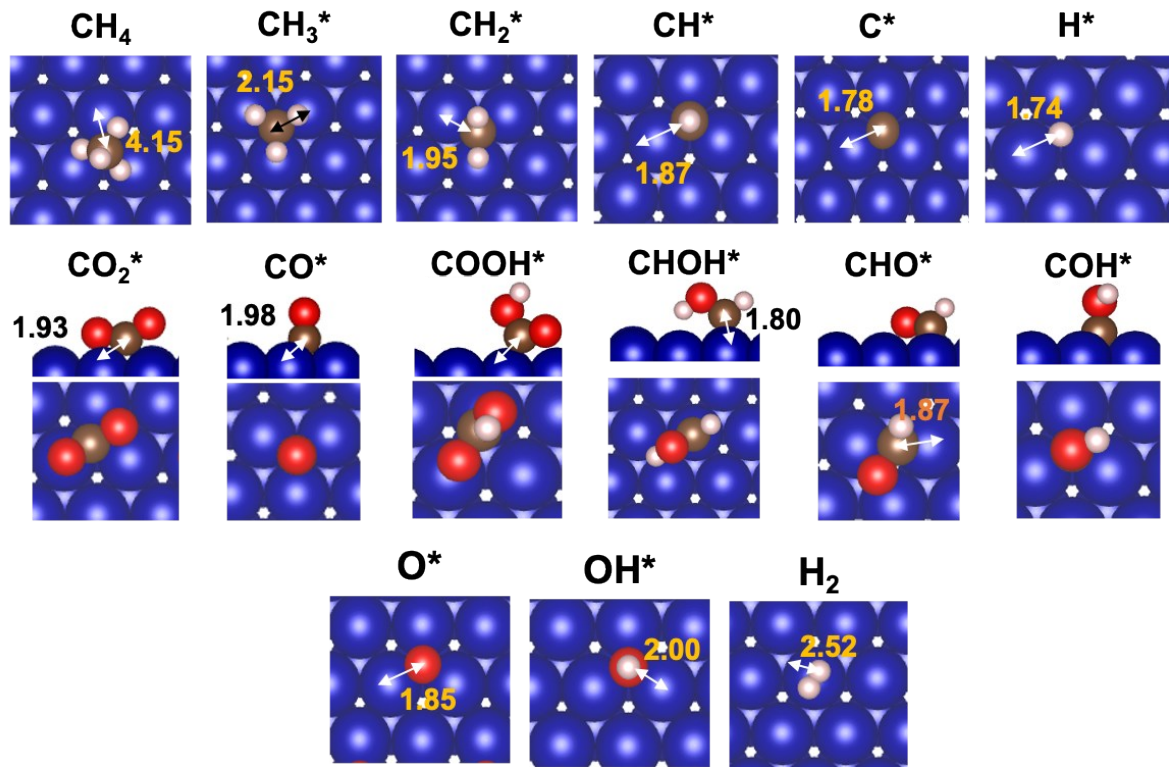


Fig. S1

Manavi and Liu

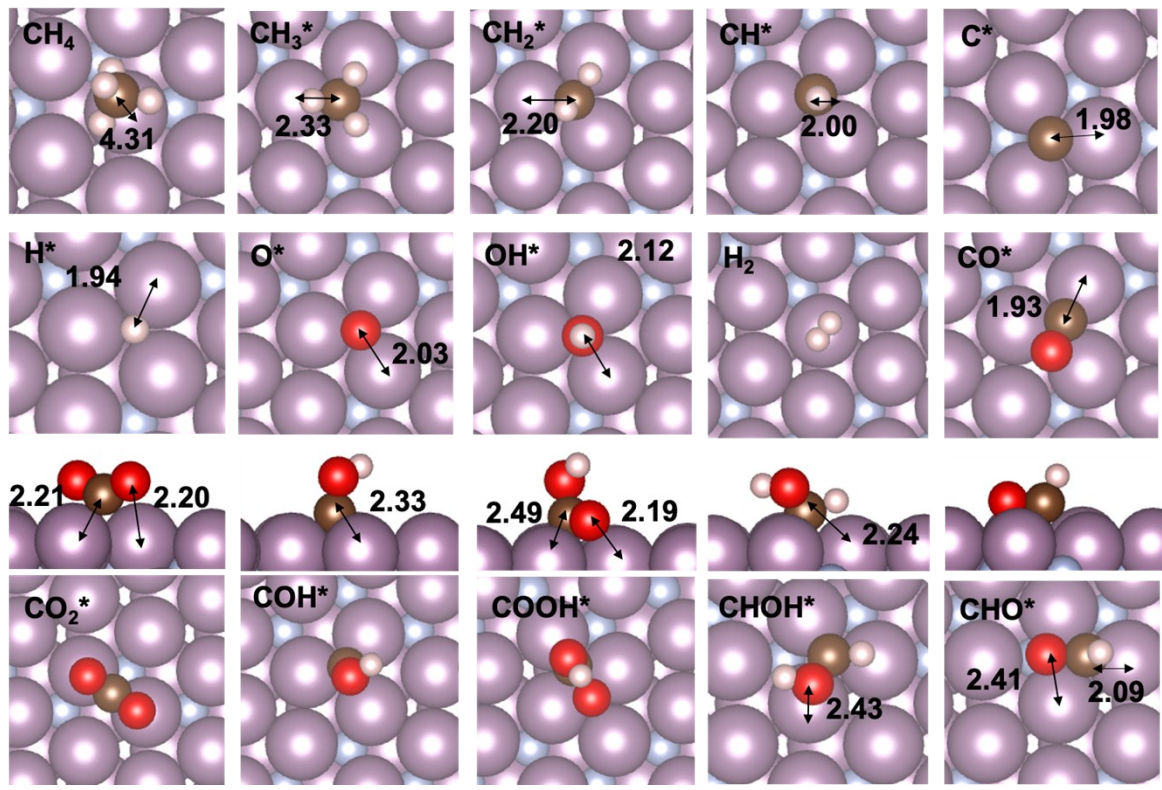


Fig. S2

Manavi and Liu

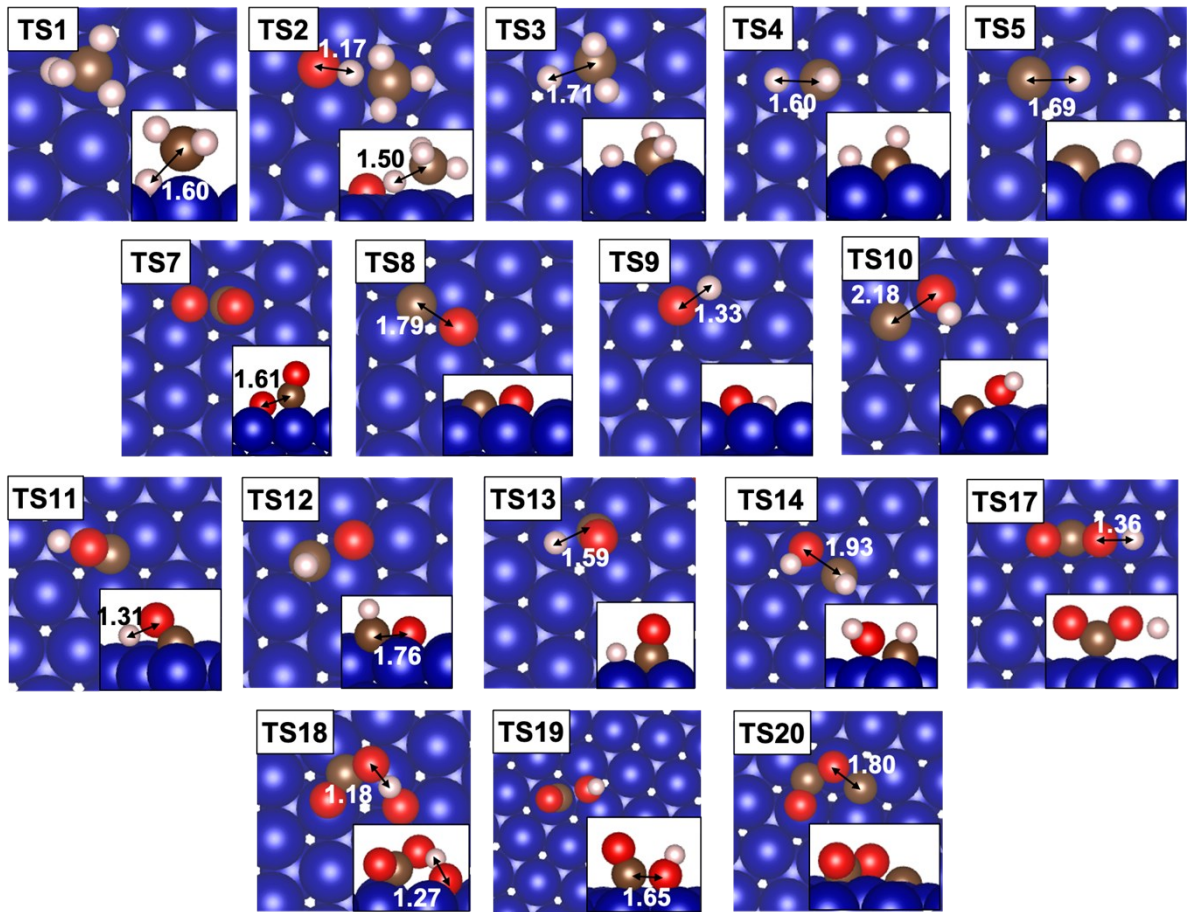


Fig. S3

Manavi and Liu

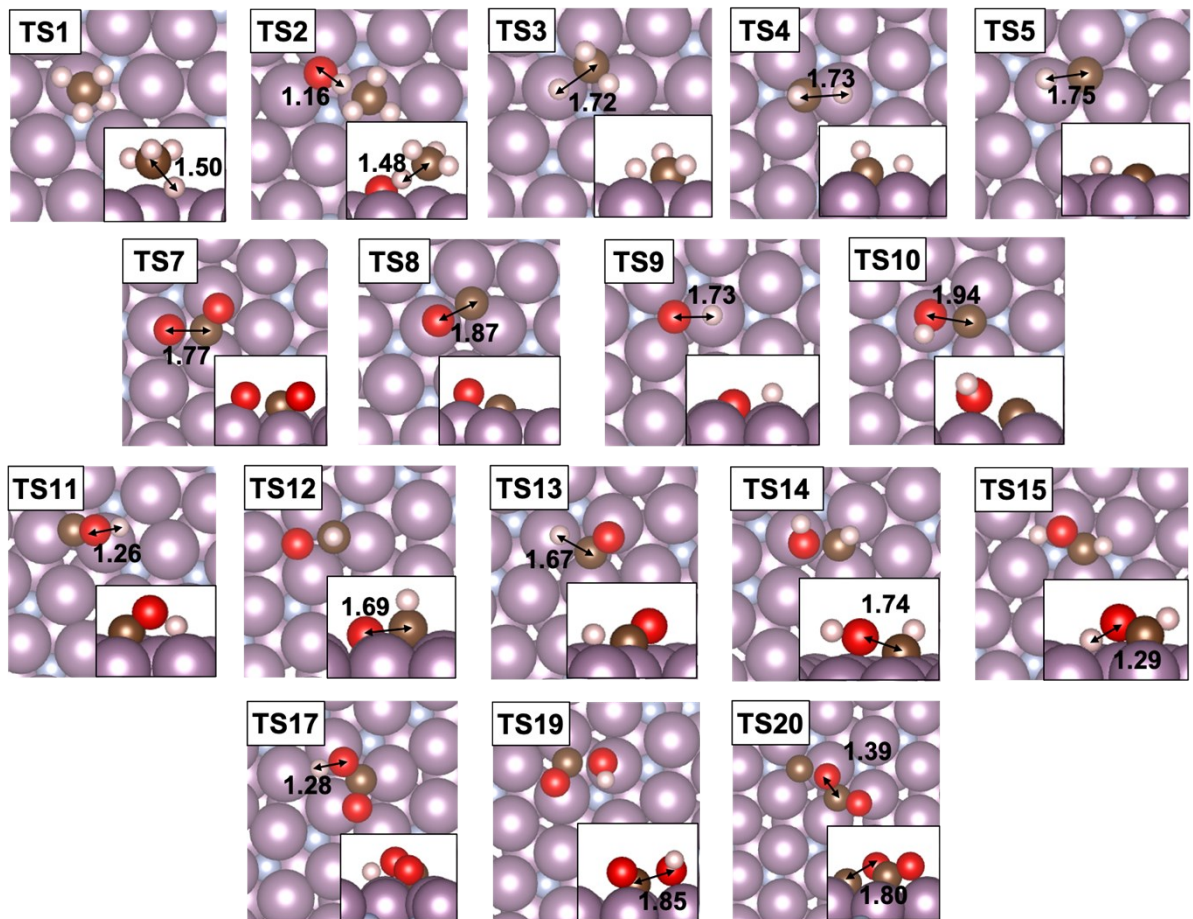


Fig. S4

Manavi and Liu

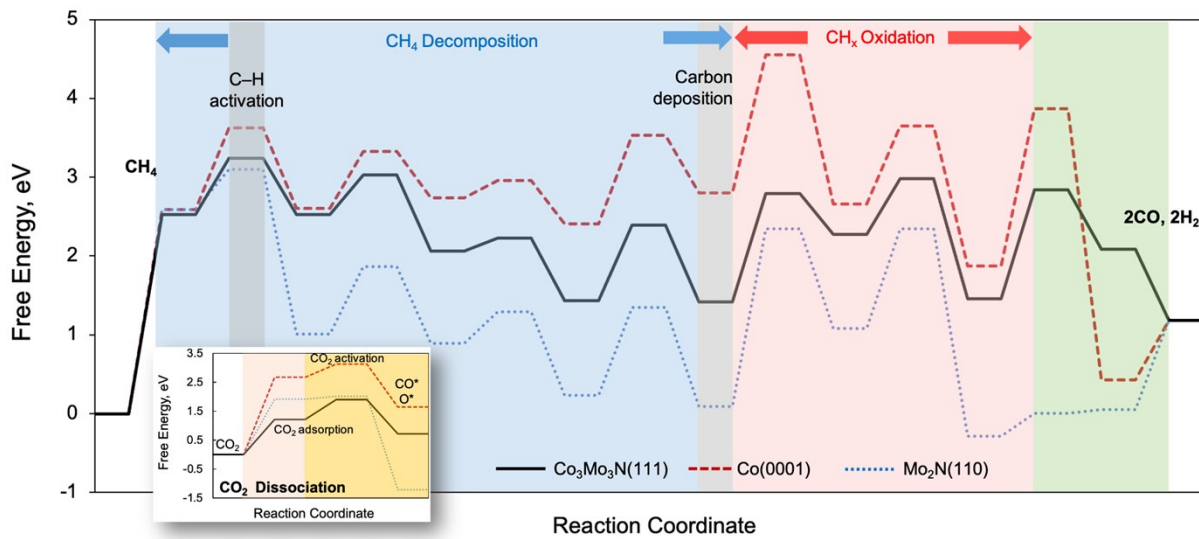


Fig. S5

Manavi and Liu

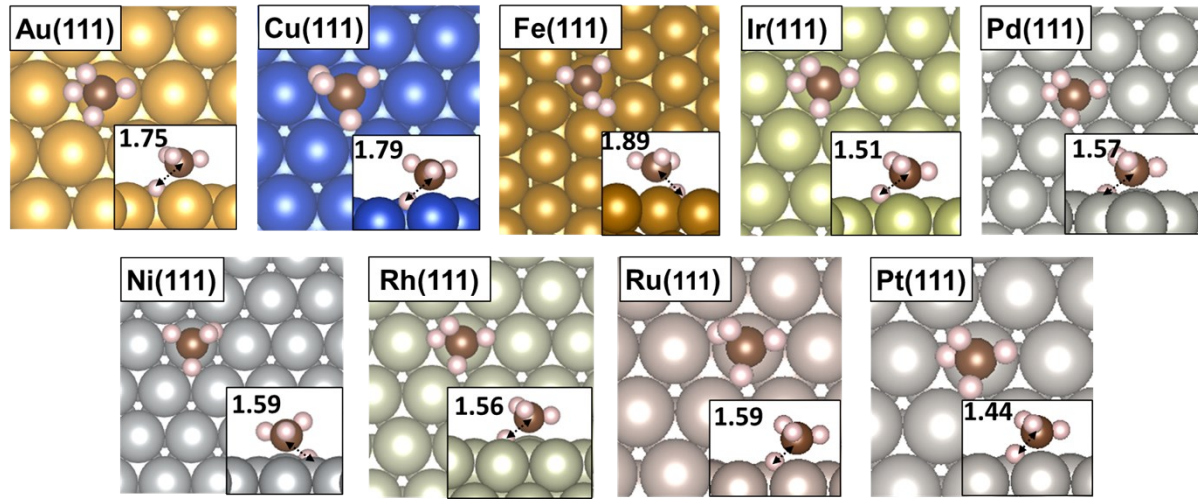


Fig. S6

Manavi and Liu

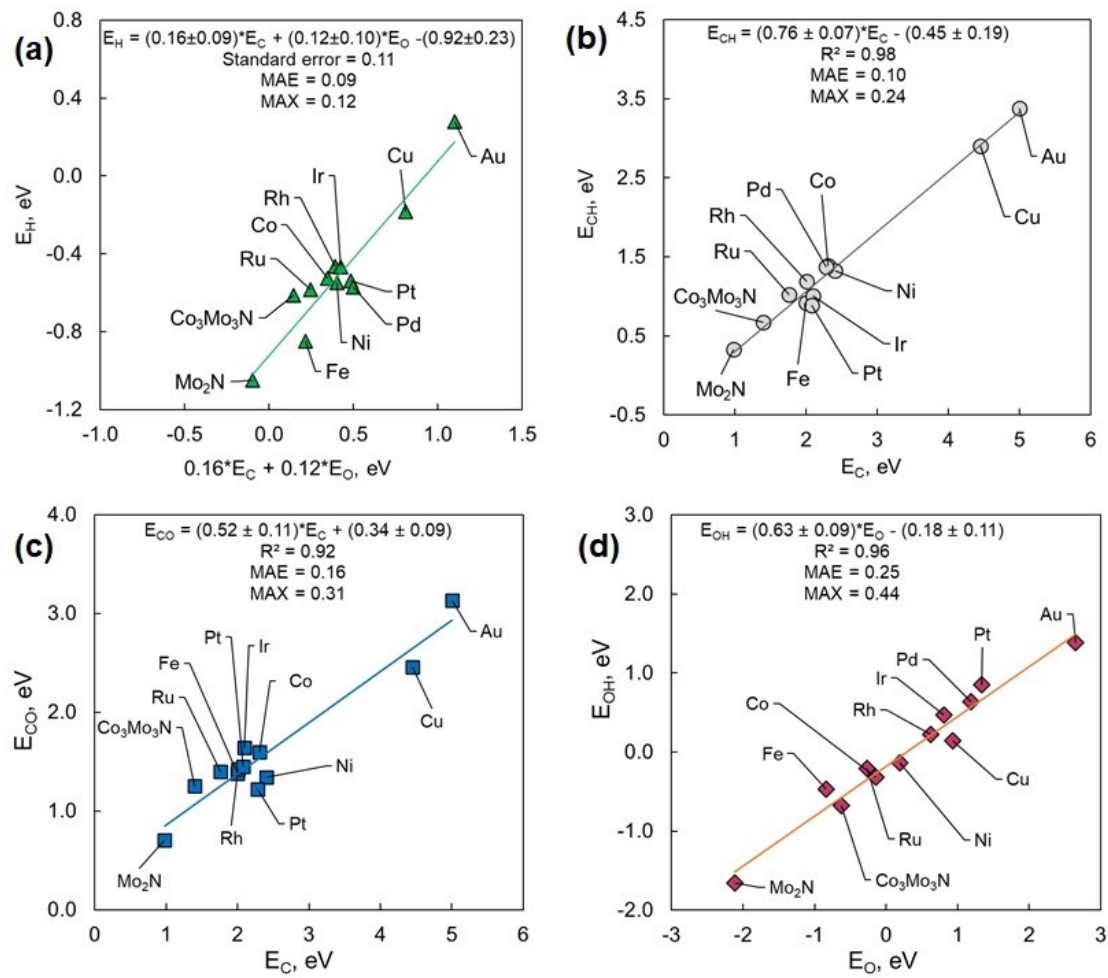


Fig. S7

Manavi and Liu

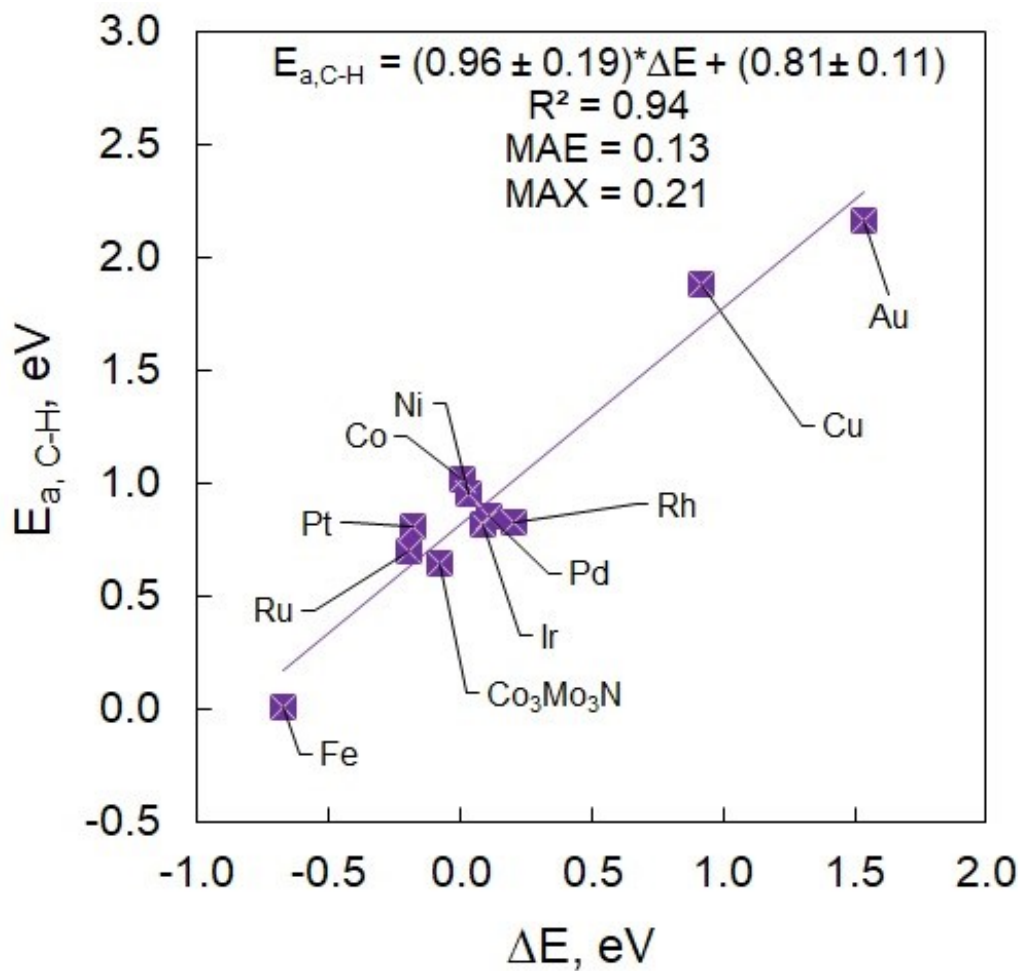


Fig. S8

Manavi and Liu

Table S1. Lattice parameters of surface models.

Surface	Lattice parameter (Å)	Experimental lattice (Å)
Co(0001)	2.476	2.501
Mo ₂ N(110)	4.999	5.044
Co ₃ Mo ₃ N(111)	7.783	7.813
Ni(111)	2.491	2.481
Pt(111)	2.804	2.812
Cu(111)	2.580	2.561
Au(111)	2.949	2.950
Ir(111)	2.714	2.741
Rh(111)	2.705	2.721
Fe(111)	2.440	2.578
Pd(111)	2.751	2.798
Ru(111)	2.711	2.705

Table S2. Binding energies (eV) of H and CH₃ and their preferred binding sites on close-packed transition metal surfaces; CH₄ dissociation energies (ΔE); and C–H bond activation energy barriers (E_a). The literature values are shown in the parentheses.

Surface	H		CH ₃		CH ₄ dissociation	
	Site	BE, eV (BE _{lit.})	Site	BE (eV) (BE _{lit.})	ΔE , eV	E_a , eV
Ir(111)	top	-2.72 (-2.73 ¹)	fcc	-1.92 (-1.88 ¹)	0.09 (0.06 ²)	0.82 (0.95 ²)
Rh(111)	fcc	-2.72 (-2.86 ³)	fcc	-1.80 (-1.84 ⁴ , -1.83 ⁵)	0.21 (0.12 ⁶ , 0.09 ³ , 0.05 ²)	0.83 (0.82 ⁶ , 0.72 ³ , 1.00 ²)
Ni(111)	fcc	-2.81 (-2.80 ⁷)	top	-1.89 (-1.91 ⁷)	0.03 (0.13 ^{8,9} , 0.01 ⁷ , 0.15 ¹⁰)	0.95 (1.18 ^{8,9} , 1.17 ¹⁰ , 0.90 ¹¹ , 0.88 ⁷)
Cu(111)	fcc	-2.44 (-2.51 ⁹)	fcc	-1.37 (-2.03 ¹²)	0.92 (1.07 ¹² , 1.25 ²)	1.88 (1.77 ¹² , 1.80 ²)
Fe(111)	hcp	-2.98	fcc	-2.29 (-2.81 ⁹)	-0.67 (-0.63 ¹⁴)	0.01
Pt(111)	top	-2.79 (-2.74 ¹³)	top	-2.10 (-2.02 ¹³)	-0.18 (-0.13 ¹⁴ , 0.07 ¹⁵ , 0.04 ²)	0.81 (0.84 ¹⁴ , 0.77 ¹⁵ , 1.10 ²)
Au(111)	fcc	-1.98	-	-1.21	1.53 (1.75 ²)	2.16 (2.25 ²)
Pd(111)	fcc	-2.82 (-2.68)	top	-1.79 (-1.81 ¹⁶)	0.11 (0.26)	0.85 (0.97)
Ru(111)	fcc	-2.84	fcc	-2.08	-0.20 (-0.23)	0.70 (0.80 ¹⁷)

Table S3. Calculated rate constants for the elementary DRM steps on Co₃Mo₃N(111), Co(0001), Mo₂N(110), and Ni(111). The elementary step indices correspond to the mechanism shown in Table 2 of the main text.

Elementary step	Co ₃ Mo ₃ N(111)		Co(0001)		Mo ₂ N(110)		Ni(111)	
	k_f	k_r	k_f	k_r	k_f	k_r	k_f	k_r
R1	1.85E-01	1.60E+13	7.28E-02	7.44E+11	1.65E+00	6.69E+05	4.01E-02	9.08E+11
R2	2.15E-02	3.40E+13	1.52E-04	9.75E+08	5.44E-07	3.27E+06	-	-
R3	6.62E+10	1.92E+08	3.78E+09	1.78E+10	8.03E+08	1.92E+08	7.46E+09	1.11E+10
R4	2.55E+10	1.39E+07	1.47E+12	2.87E+10	1.72E+11	6.56E+07	2.87E+11	3.00E+09
R5	2.44E+08	3.93E+08	2.85E+07	3.36E+09	1.53E+11	2.87E+10	1.28E+06	7.13E+08
R6	1.49E+01	7.56E+05	2.65E+02	4.79E+13	2.78E+01	2.97E+09	4.01E+02	1.63E+13
R7	5.41E+09	1.39E+07	1.35E+11	3.89E+05	6.15E+11	3.79E+03	1.58E+10	1.69E+05
R8	2.39E+02	2.53E+07	5.99E+03	6.69E+00	1.03E-01	8.26E+04	1.05E+05	2.46E-02
R9	3.33E+06	9.83E+09	5.36E+06	3.49E+08	1.00E+03	6.62E+10	1.77E+07	1.70E+08
R10	1.63E+06	4.11E+10	1.75E+04	3.30E+03	4.00E+01	5.36E+06	2.33E+06	4.72E+03
R11	4.26E+09	2.72E+05	4.42E+08	3.59E+04	5.36E+06	4.85E-01	2.44E+08	2.60E+03
R12	5.77E+04	5.03E+11	1.18E+05	5.41E+09	1.89E+02	2.37E+12	2.14E+05	8.33E+07
R13	1.72E+11	8.33E+07	1.03E+12	2.62E+06	2.35E+09	2.51E+04	2.10E+12	7.07E+05
R14	7.60E+03	8.10E+11	3.07E+05	2.01E+10	1.12E+00	1.94E+11	6.27E+05	3.79E+09
R15	3.24E+10	6.27E+05	-	-	1.53E+11	1.67E+02	4.26E+09	2.53E+07
R16	1.31E+12	2.16E+08	1.03E+12	1.34E+08	-	-	6.15E+12	1.02E+09
R17	7.96E+05	3.39E+12	8.97E+05	2.24E+07	3.09E+08	2.55E+10	7.96E+05	3.39E+12
R18	1.70E+08	2.46E+11	6.56E+07	1.57E+07	-	-	1.70E+08	2.46E+11
R19	1.07E+11	1.90E+05	1.16E+12	9.74E+06	1.31E+12	6.45E+01	1.07E+11	1.90E+05
R20	8.89E+02	1.09E+04	7.60E+03	2.44E-05	8.97E+05	4.43E-05	8.89E+02	1.09E+04
R21	2.72E+03	1.07E-02	1.62E+05	2.82E-01	4.03E+00	2.40E-02	1.68E+04	1.29E-01
R22	2.62E+07	1.82E+01	2.07E+08	2.22E+01	8.15E+02	2.00E+01	1.26E+08	9.84E+00
R23	1.22E+07	1.60E+02	2.40E+09	6.42E+02	5.71E-01	1.93E+02	1.56E+10	3.38E+02

Appendix 1. Derivation of single-site and dual-site microkinetic models for DRM

All elementary steps are generally described by Eqn. (S1),



where $AB^\#$ represents the activated transition state. According to Eqn. (S2), the rate constants (k) becomes:

$$k = \frac{k_B T}{h} \exp\left(\frac{-E_a}{RT}\right), \quad (S2)$$

where k_B is the Boltzmann constant, h is the Planck's constant, R is the gas constant (i.e., 8.314 J/K mole), and T is temperature (in K). All E_a were obtained from DFT CI-NEB and dimer calculations detailed in the main text.

Specifically, the forward and reverse rate constants for the rate-determining CH_4 dissociative adsorption are expressed by Eqns. (S3-S4):

$$k_f = \frac{k_B T}{h} \frac{q^\#}{q_{\text{CH}_4(g)}} \exp\left(-\frac{E_{af}}{RT}\right), \quad (S3)$$

$$k_r = \frac{k_B T}{h} \frac{q^\#}{q_{\text{CH}_3^*} q_{\text{H}^*}} \exp\left(-\frac{E_{ar}}{RT}\right), \quad (S4)$$

where q_{TS} , q_{CH_4} , q_{surf} , $q_{\text{CH}_3^*}$, and q_{H^*} are the partition functions for the transition state (TS), the reactant, and product states with respect to their ground states, respectively. These partition functions were estimated based on the standard statistical mechanical approach at 1 bar and 973.15 K.

E_{af} and E_{ar} , with zero-point energy (ZPE) corrections included, correspond to the activation energies of the forward and reverse elementary step, respectively.

For molecular adsorption and desorption process (e.g., CO₂ adsorption), as expressed by Eqn. (S5),



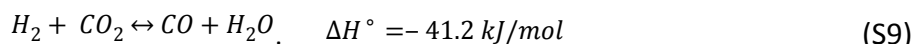
It can be shown that the rate constants for molecular adsorption and desorption can be expressed by Eqns. (S6) and (S7)¹⁸:

$$k_{adsorption} = \frac{1}{N_0 \sqrt{2\pi k_B T M_A}} q_{r_{A(g)}} q_{v_{A(g)}}^{q_{A^*}} \quad (S6)$$

$$k_{desorption} = e \frac{k_B T}{h} \exp \left(-\frac{\Delta E}{RT} \right) \quad (S7)$$

where N_0 is the number of surface sites of the exposed surface. M_A is the molecular mass of the adsorbate (A). $q_{r_{A(g)}}$ and $q_{v_{A(g)}}$ are the rotational and vibrational partition functions of the gas-phase adsorbate, respectively. ΔE is approximated with the binding energy of the adsorbate.

A *Mathematica* script was developed to obtain the DRM turnover frequencies (TOFs) and surface coverage at $P = 1$ bar and 973.15 K. The initial feed consists of equimolar CH₄ and CO₂ (i.e., $p_{CH_4} = p_{CO_2} = 0.5$ bar) at a molar flow rate of 1 mole/s. The composition for the exiting gas stream consisting of CO, H₂ and H₂O, and the unreacted CH₄, CO₂, was estimated based on the overall equilibrium constant. The relevant reactions consist of the DRM (S8) and the reverse water-gas shift reaction (S9):



The estimated equilibrium constants at 1 bar and 973.15 K are 5.92 and 0.594, respectively. Hence, thermodynamics will favor DRM strongly over the reverse water-gas shift

reaction at high temperatures. The composition of the exiting gas stream were determined with Eqns. (S10) and (S11):

$$K_{DRM}(T) = \frac{\left(\frac{p_{H_2}}{P}\right)_2 \left(\frac{p_{CO}}{P}\right)_2}{\left(\frac{p_{CH_4}}{P}\right) \left(\frac{p_{CO_2}}{P}\right)}, \quad (S10)$$

$$K_{RWGS}(T) = \frac{p_{H_2} * p_{CO_2}}{p_{CO} * p_{H_2O}}, \quad (S11)$$

where the partial pressures are represented by Eqns. (S12-S16) in terms of CH_4 conversion (x_{CH_4}) and the extent of reaction of RWGS (ξ).

$$p_{CH_4} = \frac{1 - x_{CH_4}}{2 * (1 + x_{CH_4})} P \quad (S12)$$

$$p_{CO_2} = \frac{1 - x_{CH_4} * \xi}{2 * (1 + x_{CH_4})} P \quad (S13)$$

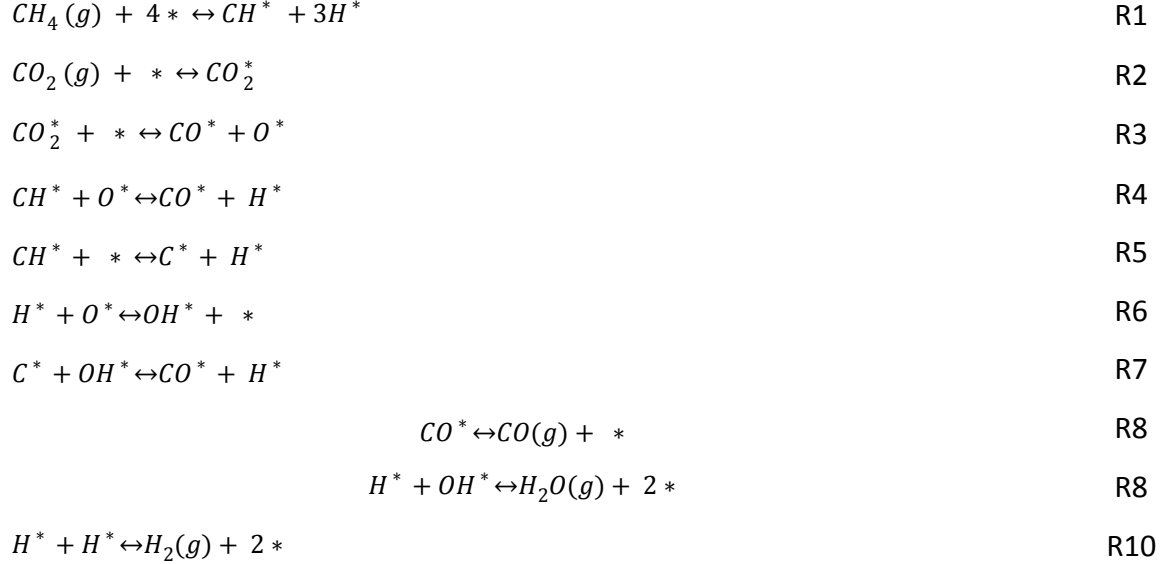
$$p_{CO} = \frac{2 * F_0 * x_{CH_4} + \xi}{2 * F_0 * (1 + x_{CH_4})} P \quad (S14)$$

$$p_{CO} = \frac{2 * F_0 * x_{CH_4} - \xi}{2 * F_0 * (1 + x_{CH_4})} P \quad (S15)$$

$$p_{H_2O} = \frac{\xi}{2 * F_0 * (1 + x_{CH_4})} P \quad (S16)$$

As mentioned in the main text, a reduced DRM mechanism was adopted to facilitate microkinetic modeling. The first activation of CH_4 was still treated as the rate-limiting step (RLS) and will be used to determine the rate of DRM. In addition, the CH_4 decomposition sequence was represented as a *lumped* step (forming CH , see R), by neglecting the formation and oxidations of CH_2 and CH_3 . Because the formation of $CHOH$ is significantly slower (see Table S4),

the CHO intermediate will be omitted. Instead, the oxidation of carbonaceous species (i.e., C and CH) is represented by R4 and R7, to form CO. The oxidants (i.e., O and OH) are generated via R3 and R6, respectively. Hence, there are 10 elementary steps, involving 5 gas phase species (CH_4 , CO_2 , CO, H₂, and H₂O) and 8 surface intermediates (*, C, CH, CO_2^* , CO, O, H, and OH) in the reduced DRM model.



The quasi-steady state assumption (QSSA) was applied to each surface species (excluding vacancies) in order to establish a set of differential equations describing each surface species, as in Eqns. (S17-S24):

$$r_1 = k_{1f}P_{\text{CH}_4}\theta_*^4 - k_{1r}\theta_{\text{CH}}\theta_H^3 \quad (\text{S17})$$

$$\frac{d\theta_{\text{CO}_2}}{dt} = k_{2f}P_{\text{CO}_2}\theta_* - k_{2r}\theta_{\text{CO}_2} \quad (\text{S18})$$

$$\frac{d\theta_O}{dt} = k_{3f}\theta_{\text{CO}_2}\theta_* - k_{3r}\theta_{\text{CO}}\theta_O \quad (\text{S19})$$

$$\frac{d\theta_{\text{CH}}}{dt} = -k_{4f}\theta_{\text{CH}}\theta_O + k_{4r}\theta_{\text{CO}}\theta_H - k_{5f}\theta_{\text{CH}}\theta_* + k_{5r}\theta_C\theta_H \quad (\text{S20})$$

$$\frac{d\theta_{\text{OH}}}{dt} = k_{6f}\theta_O\theta_H + k_{6r}\theta_{\text{OH}}\theta_* \quad (\text{S21})$$

$$\frac{d\theta_C}{dt} = -k_{7f}\theta_C\theta_{OH} + k_{7r}\theta_{CO}\theta_H \quad (S22)$$

$$\frac{d\theta_{CO}}{dt} = -k_{8f}\theta_{CO} + k_{8r}P_{CO}\theta_* \quad (S23)$$

$$\frac{d\theta_H}{dt} = -k_{9f}\theta_{OH}\theta_H + k_{9r}P_{H_2O}\theta_*^2 - k_{10f}\theta_H^2 + k_{10r}P_{H_2}\theta_*^2 \quad (S24)$$

The rate constants corresponding to the above model are listed in Table S5.

Table S4. Rate constants and equilibrium constants on Co₃Mo₃N(111), Ni(111), Co(0001), and Mn₂N(110) used in Eqns. (S3, S4, S6, S7).

Elementary step	Co ₃ Mo ₃ N(111)			Ni(111)		
	k _{fi}	k _{ri}	K _i	k _{fi}	k _{ri}	K _i
R1	1.85E-01	1.39E+07	1.33E-08	4.00E-02	3.00E+9	3.33E-11
R2	1.48E+01	7.57E+05	1.96E-05	4.01E+02	1.63E+13	2.46E-11
R3	5.41E+09	1.39E+07	3.89E+02	1.58E+10	1.69E+05	9.35E+04
R4	5.77E+04	8.33E+07	6.92E-04	2.14E+05	7.07E+05	3.03E-01
R5	2.44E+08	3.93E+08	6.21E-01	1.28E+06	7.13E+08	1.80E-03
R6	3.33E+06	9.83E+09	3.39E-04	1.77E+07	1.70E+08	1.04E-01
R7	1.63E+06	2.72E+05	5.99E+00	2.33E+06	2.60E+03	8.96E+02
R8	2.72E+03	1.07E-02	2.54E+05	1.68E+04	1.28E-01	1.31E+05
R9	1.22E+07	1.60E+02	7.63E+04	1.56E+10	3.38E+02	4.62E+07
R10	2.62E+07	1.82E+01	1.44E+06	1.25E+08	9.84E+00	1.27E+07
Elementary step	Co(0001)			Mo ₂ N(110)		
	k _{fi}	k _{ri}	K _i	k _{ri}	K _i	
R1	7.28E-02	1.78E+09	4.09E-11	1.65E+00	6.69E+05	2.46E-06
R2	1.00E+00	4.79E+13	2.09E-12	2.78E+01	2.97E+09	9.36E-09
R3	1.35E+11	3.89E+05	3.47E+05	6.15E+12	3.79E-04	1.62E+16
R4	1.18E+05	2.62E+06	4.50E-02	1.89E+02	2.51E+04	7.53E-03
R5	2.85E+07	3.36E+09	8.48E-03	1.53E+11	2.87E+10	5.33E+00
R6	5.36E+06	3.49E+08	1.54E-02	1.00E+03	6.62E+10	1.51E-08
R7	1.75E+04	3.30E+02	5.30E+01	4.00E+01	4.85E-01	8.25E+01
R8	1.62E+05	2.82E-01	5.74E+06	4.03E+00	2.40E-02	1.68E+02
R9	2.40E+09	6.42E+02	3.74E+06	5.70E-01	1.93E+02	2.95E-03
R10	2.07E+08	2.22E+01	9.32E+06	8.15E+02	2.00E+01	4.08E+01

According to QSSA, the surface coverage expressions are represented by Eqns. (S25-S32 in Table S5) for the *single-site* mechanism.

<i>Single-site mechanism</i>		<i>Dual-site mechanism</i>
(S25)	$\theta_{CO_2} = K_2 p_{CO_2} \theta_*$	(S43) $\theta_{CO_2} = K_2 p_{CO_2} \theta_{1*}$
(S26)	$\theta_O = \frac{K_3 \theta_{CO_2} \theta_*}{\theta_{CO}} = \frac{K_2 K_3 K_8 p_{CO_2}}{p_{CO}} \theta_*$	(S44) $\theta_O = \frac{K_3 \theta_{CO_2} \theta_{2*}}{\theta_{CO}} = \frac{K_2 K_3 K_8 p_{CO_2}}{p_{CO}} \theta_{2*}$
(S27)	$\theta_{CH} = \frac{\frac{k_{4r} p_{CO}}{K_8} + \frac{k_{5r} p_{CO}^2}{K_2 K_3 K_6 K_7 K_8^2 p_{CO_2}}}{\frac{k_{4f} K_2 K_3 K_8 p_{CO_2}}{p_{CO}} + k_{5f}} \times \sqrt{\frac{\frac{k_{9r} p_{H_2} + k_{10r} p_{H_2}}{K_2 K_3 K_6 K_8 k_{9f} p_{CO_2}}}{\frac{k_{9r} p_{H_2} + k_{10r} p_{H_2}}{p_{CO}} + k_{10f}} \theta_*}$	(S45) $\theta_{CH} = \frac{\frac{k_{4r} p_{CO}}{K_8} \theta_{2*} + \frac{k_{5r} p_{CO}^2}{K_2 K_3 K_6 K_7 K_8^2 p_{CO_2}} \theta_{1*}}{\frac{k_{4f} K_2 K_3 K_8 p_{CO_2}}{p_{CO}} + k_{5f}} \sqrt{\frac{\frac{k_{9r} p_{H_2} + k_{10r} p_{H_2}}{K_2 K_3 K_6 K_8 k_{9f} p_{CO_2}}}{\frac{k_{9r} p_{H_2} + k_{10r} p_{H_2}}{p_{CO}} + k_{10f}} \theta_{2*}}$
(S28)	$\theta_{OH} = \frac{K_2 K_3 K_6 K_8 p_{CO_2}}{p_{CO}} \times \sqrt{\frac{\frac{k_{9r} p_{H_2} + k_{10r} p_{H_2}}{K_2 K_3 K_6 K_8 k_{9f} p_{CO_2}}}{\frac{k_{9r} p_{H_2} + k_{10r} p_{H_2}}{p_{CO}} + k_{10f}} \theta_*}$	(S46) $\theta_{OH} = \frac{K_2 K_3 K_6 K_8 p_{CO_2}}{p_{CO}} \sqrt{\frac{\frac{k_{9r} p_{H_2} + k_{10r} p_{H_2}}{K_2 K_3 K_6 K_8 k_{9f} p_{CO_2}}}{\frac{k_{9r} p_{H_2} + k_{10r} p_{H_2}}{p_{CO}} + k_{10f}} \theta_{2*}}$
(S29)	$\theta_C = \frac{\theta_{CO} \theta_H}{K_7 \theta_{OH}} = \frac{p_{CO}^2}{K_2 K_3 K_6 K_7 K_8^2 p_{CO_2}} \theta_*$	(S47) $\theta_C = \frac{\theta_{CO} \theta_H}{K_7 \theta_{OH}} = \frac{p_{CO}^2}{K_2 K_3 K_6 K_7 K_8^2 p_{CO_2}} \theta_{1*}$
(S30)	$\theta_{CO} = \frac{p_{CO}}{K_8} \theta_*$	(S48) $\theta_{CO} = \frac{p_{CO}}{K_8} \theta_{1*}$
(S31)	$\theta_H = \sqrt{\frac{\frac{k_{9r} p_{H_2} + k_{10r} p_{H_2}}{K_2 K_3 K_6 K_8 k_{9f} p_{CO_2}}}{\frac{k_{9r} p_{H_2} + k_{10r} p_{H_2}}{p_{CO}} + k_{10f}} \theta_*}$	(S49) $\theta_H = \sqrt{\frac{\frac{k_{9r} p_{H_2} + k_{10r} p_{H_2}}{K_2 K_3 K_6 K_8 k_{9f} p_{CO_2}}}{\frac{k_{9r} p_{H_2} + k_{10r} p_{H_2}}{p_{CO}} + k_{10f}} \theta_{2*}}$

(S32)	$\theta_* + \theta_C + \theta_{CH} + \theta_{CO} + \theta_{CO_2} + \theta_O + \theta_{OH} + \theta_H$	(S50) $\theta_{1*} + \theta_C + \theta_{CO} + \theta_{CO_2} = 0.7$
		(S51) $\theta_{2*} + \theta_O + \theta_{OH} + \theta_H + \theta_{CH} = 0.3$

The concentrations of all surface species are related to θ_* . Then, the RLS (r_1) can be expressed by Eqn. (S33).

$$r_1 = k_{1f} p_{CH_4} \left[1 - \frac{\frac{k_{4r} p_{CO}}{K_8} + \frac{k_{5r} p_{CO}^2}{K_2 K_3 K_6 K_7 K_8^2 p_{CO_2}}}{K_1 p_{CH_4} \left(\frac{k_{4f} K_2 K_3 K_8 p_{CO_2}}{p_{CO}} + k_{5f} \right)} \left(\frac{k_{9r} p_{H_2O} + k_{10r} p_{H_2}}{K_2 K_3 K_6 K_8 k_{9f} p_{CO_2} + k_{10f}} \right)^2 \right] \theta_*^4 \quad (S33)$$

From a dimensional analysis, the RLS can be further simplified as Eqn. (S34):

$$r_1 = k_{1f} p_{CH_4} \theta_*^4 \left[1 - \frac{p_{CO}^2 p_{H_2}^2}{K_1 K_2 K_3 K_5 K_6 K_7 K_8^2 p_{CH_4} p_{CO_2}} \right] \quad (S34)$$

The *dual-site* mechanism accounts for DRM occurring on two distinct active sites, denoted as θ_{1*} and θ_{2*} , as established by Eqns. (S35-S42). We assumed that each species occupies their preferred binding sites and the diffusions between different active domains be neglected. The surface coverage for each intermediate are represented by Eqns. (S43-S51) listed in Table S5.

$$r_1 = k_{1f} P_{CH_4} \theta_{1*}^4 - k_{1r} \theta_{CH} \theta_H^3 \quad (S35)$$

$$\frac{d\theta_{CO_2}}{dt} = k_{2f} P_{CO_2} \theta_{2*} - k_{2r} \theta_{CO_2} \quad (S36)$$

$$\frac{d\theta_O}{dt} = k_{3f} \theta_{CO_2} \theta_{1*} - k_{3r} \theta_{CO} \theta_O \quad (S37)$$

$$\frac{d\theta_{CH}}{dt} = -k_{4f} \theta_{CH} \theta_O + k_{4r} \theta_{CO} \theta_H - k_{5f} \theta_{CH} \theta_{1*} + k_{5r} \theta_C \theta_H \quad (S38)$$

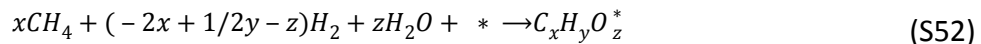
$$\frac{d\theta_{OH}}{dt} = k_{6f} \theta_O \theta_H + k_{6r} \theta_{OH} \theta_{2*} \quad (S39)$$

$$\frac{d\theta_C}{dt} = -k_{7f}\theta_C\theta_{OH} + k_{7r}\theta_{CO}\theta_H \quad (S40)$$

$$\frac{d\theta_{CO}}{dt} = -k_{8f}\theta_{CO} + k_{8r}P_{CO}\theta_{1*} \quad (S41)$$

$$\frac{d\theta_H}{dt} = -k_{9f}\theta_{OH}\theta_H + k_{9r}P_{H_2O}\theta_{2*}^2 - k_{10f}\theta_H^2 + k_{10r}P_{H_2O}\theta_{2*}^2 \quad (S42)$$

The heat map contour plot was generated using BE_C and BE_O , which are in general ($C_xH_yO_z^*$) defined by Eqns. (S52-S53).



$$E_{C_xH_yO_z^*} = E_{C_xH_yO_z^*}^{vasp} - xE_{CH_4}^{vasp} + (2x - 1/2y + z)E_{H_2}^{vasp} - zE_{H_2O}^{vasp} - E_*^{vasp} \quad (S53)$$

Then, the binding energies of H, CH, CO, and OH were estimated using Eqns. S54-S57. These linear scaling relationships were established and illustrated in Figure S7. Moreover, the C–H bond activation energies were estimated using a BEP relationship based on Eqn. S58 (also see Figure S8).

$$BE_H = 0.16BE_C + 0.12BE_O - 0.92 \quad (S54)$$

$$BE_{CH} = 0.76 BE_C - 0.45 \quad (S55)$$

$$BE_{CO} = 0.52 BE_C + 0.34 \quad (S56)$$

$$BE_{OH} = 0.63 BE_O - 0.18 \quad (S57)$$

$$E_{a,C-H} = 0.96 \Delta E + 0.81 = 0.96 (BE_{CH} + 3BE_H) + 0.81 \quad (S58)$$

Notes and references

1. W. P. Krekelberg, J. Greeley and M. Mavrikakis, *The Journal of Physical Chemistry B*, 2004, **108**, 987-994.
2. D. Hibbitts and M. Neurock, *Surface Science*, 2016, **650**, 210-220.
3. B. S. Bunnik and G. J. Kramer, *Journal of Catalysis*, 2006, **242**, 309-318.
4. M. Mavrikakis, J. Rempel, J. Greeley, L. B. Hansen and J. K. Nørskov, *The Journal of Chemical Physics*, 2002, **117**, 6737-6744.

5. H. Xiao and D. Xie, *Surface Science*, 2004, **558**, 15-22.
6. B. Wang, L. Song and R. Zhang, *Applied Surface Science*, 2012, **258**, 3714-3722.
7. Z. Wang, X. M. Cao, J. Zhu and P. Hu, *Journal of Catalysis*, 2014, **311**, 469-480.
8. H. Liu, R. Yan, R. Zhang, B. Wang and K. Xie, *Journal of Natural Gas Chemistry*, 2011, **20**, 611-617.
9. H. Liu, B. Wang, M. Fan, N. Henson, Y. Zhang, B. F. Towler and H. G. Harris, *Fuel*, 2013, **113**, 712-718.
10. S.-G. Wang, X.-Y. Liao, J. Hu, D.-B. Cao, Y.-W. Li, J. Wang and H. Jiao, *Surface Science*, 2007, **601**, 1271-1284.
11. Y.-A. Zhu, D. Chen, X.-G. Zhou and W.-K. Yuan, *Catalysis Today*, 2009, **148**, 260-267.
12. T. Niu, Z. Jiang, Y. Zhu, G. Zhou, M. A. van Spronsen, S. A. Tenney, J. A. Boscoboinik and D. Stacchiola, *The Journal of Physical Chemistry B*, 2018, **122**, 855-863.
13. A. Trinchero, A. Hellman and H. Grönbeck, *Surface Science*, 2013, **616**, 206-213.
14. Q. Qi, X. Wang, L. Chen and B. Li, *Applied Surface Science*, 2013, **284**, 784-791.
15. R. Zhang, L. Song and Y. Wang, *Applied Surface Science*, 2012, **258**, 7154-7160.
16. C.-Q. Lv, K.-C. Ling and G.-C. Wang, *The Journal of Chemical Physics*, 2009, **131**, 144704.
17. X. Wang, Q. Yuan, J. Li and F. Ding, *Nanoscale*, 2017, **9**, 11584-11589.
18. I. Chorkendorff, J. W. Niemantsverdriet, W. John and Sons, *Concepts of modern catalysis and kinetics*, Wiley-VCH, 2003.